Heliyon 10 (2024) e31674

Contents lists available at ScienceDirect

Heliyon

journal homepage: www.cell.com/heliyon

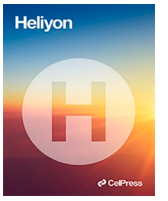

Research article

A nanocarrier system based on CQDs for efficient mitoxantrone drug delivery

Shahrzad Raeispour, Moones Rahmandoust *, Hasan Kouchakzadeh **

Protein Research Center, Shahid Beheshti University, Velenjak, 1983969411, Tehran, Iran

ARTICLE INFO

Keywords:
Carbon quantum dots (CQDs)
Mitoxantrone (MTX)
Targeted delivery
In vitro study
Breast cancer

ABSTRACT

Cancer is the second most fatal disease among women. In recent years, utilizing strategies based on carbon quantum dots (CQDs) as targeted drug delivery systems has had a significant impact on advancing and improving cancer treatment. This study is focused on the development of a nanocarrier, based on CQDs, for improving the therapeutic efficiency of mitoxantrone (MTX). Hence, the N-doped CQDs were synthesized by a hydrothermal method. Following its purification, MTX was loaded to the CQD, resulting in an increase in the size from 36.78 ± 0.9 nm to 157.8 ± 12.18 nm, with an ideal drug entrapment efficiency of 97 %. Drug release investigation showed a pH-dependent improvement, from 8 % at pH 7.4 to 11 % at pH 5.2 after 48 h. Based on the Methylthiazolyldiphenyl-tetrazolium bromide (MTT) results after 5 h of treatment on MCF-7 breast cancer cells, the N-doped CQD showed no significant effect on the cancer cells, whereas a half maximal Inhibitory Concentration (IC_{50}) was achieved with the N-doped CQD-MTX complex at a concentration between 0.5 to 0.8 μM. Therefore, the newly developed drug delivery complex was capable of providing a rather identical influence on MCF-7 cells, as the free MTX, however, improving the pharmacokinetic of the drug by its controlled and on-target drug release, due to an alteration in distribution and absorption parameters.

1. Introduction

Cancer is one of the most fatal health risks in today's societies, and extensive efforts are being made to combat it. For many years, breast cancer has had the highest incidence of all cancers in women worldwide [1]. Although recent advances in treatment techniques have significantly increased the survival rate, unfortunately, many side effects for the common treatment strategies. For instance, chemotherapy is a type of cancer treatment that uses one or more anti-cancer drugs, which usually leads to the destruction of healthy cells and cancer cells. In effect, the clinical use of anticancer drugs is limited. Targeted drug delivery has been proposed as a tool to effectively deliver drugs with high specificity to the targeted cells that leads to significantly less toxicity to healthy cells than conventional chemotherapy [2].

Among various targeted drug delivery techniques, the use of nanoparticles as drug carriers has shown to be an effective method to address various pharmacokinetic factors of the drugs in the treatment of cancer, through active and passive targeting. In passive targeting, the nanoparticle-based drug delivery system has a sensitivity to the temperature and pH of the tumor environment, which

* Corresponding author.
** Corresponding author.
E-mail addresses: shahrzad.raiespour@gmail.com (S. Raeispour), rahmandoust.moones@gmail.com (M. Rahmandoust), h_kouchakzadeh@sbu.ac.ir (H. Kouchakzadeh).

https://doi.org/10.1016/j.heliyon.2024.e31674
Received 27 January 2024; Received in revised form 20 May 2024; Accepted 20 May 2024
Available online 23 May 2024

are different from healthy cells or tissues [3,4]. In contrast, in active targeting, the drug delivery system is based on targeting the tumor environment by ligands or receptors on the surface of cancer cells, which, have higher expression levels, compared to the healthy cells, therefore, leading to higher specificity and therapeutic efficiency. Enhanced permeability and retention (EPR) in cancer treatment is another key mechanism that enables higher drug accumulation at the tumor site due to the small size, higher surface-to-volume ratio, greater reactivity, and stronger absorption of the nanoparticle-based drug delivery systems to tumor cells [5]. As a result of targeted drug delivery, different pharmacokinetic factors of the drugs are influenced, which consequently increases the effectiveness of the drug and decreases the side effects of the drugs on healthy cells and tissues.

Among various nanoparticles, carbon quantum dots (CQDs) are a class of nanoparticles that have high biocompatibility, low toxicity, and good dispersion in water [4,6]. CQDs are used for example, as drug delivery systems, transferring genes and pathogenic drugs to target cells. The mitoxantrone (MTX) drug is a type of anti-cancer drug that produces a delay in the S phase of the cell cycle. This drug mainly acts on DNA, causing a break in DNA strands by stabilizing the cleavable DNA-topoisomerase complex and producing free radicals. Moreover it causes DNA accumulation and condensation through electrostatic cross-linking [7]. MTX drug has also been used as one of the most effective agents for the treatment of relapsing-remitting, progressive-relapsing, and secondary progressive multiple sclerosis by slowing down the worsening of neurological disability [8].

MTX has been used with various nanoparticles to improve different pharmacokinetic factors. In studies conducted by Hashemi *et al.*, a system containing MTX which is loaded into poly lactic-*co*-glycolic acid (PLGA) nanoparticles was created. The percentage of drug entrapment efficiency (DEE) was 68 %. Also, at pH 7.4 after 48 h, the percentage of cumulative release of MTX from PLGA was about 30 %, while, at pH 5.5 after 48 h, it was about 60 % [9]. Based on the study conducted by Wang *et al.*, MTX-preloaded phospholipid-amorphous calcium carbonate hybrid nanoparticles (PL-ACC-MTX) that surface modified with PL shell (containing shielding polymer polyethylene glycol (PEG) and targeting moiety folic acid) were prepared. The percentage of DEE of PL-ACC-MTX was 91.36 %. Also, the percentage of cumulative release of PL-ACC-MTX in phosphate buffer of pH 7.4 was 21 % after about 48 h, while at pH 5.5, 30.3 % of the MTX was released after about 48 h [3].

In studies performed by Darwish *et al.*, two kinds of nanoparticles (chitosan and chitosan-hexagonal gold) loaded with MTX were prepared. The percentages of DEE of chitosan-MTX and chitosan-hexagonal gold-MTX were 23.6 $\pm$ 1.8 % and 18.5 $\pm$ 1.7 %, respectively. The percentages of released MTX from chitosan-MTX after 48 h were about 45 % and 67 % at pH 7.4 and 5.2, respectively, while, the release rates from chitosan-hexagonal gold-MTX after 48 h were 34 % and 55 % at pH 7.4 and 5.2, respectively [10].

Considering previously published literature, the influence of the nanoparticles on the pharmacokinetic properties of the MTX is confirmed, however, improved drug loading and release using novel particles that have high biocompatibility, low toxicity and good dispersion in water is required for safe cancer therapy. The CQDs, along with the mentioned properties, have the potential of preventing the growth of cancer cells by stabilizing the cleavable DNA-topoisomerase complex and producing free radicals. Furthermore, the free radicals generate in healthy cells, also, they damage healthy and cancerous cells through reaction with other cellular components [11,12]. In summary, the aim of this study is to design a nanocarrier system based on CQDs for efficient MTX cancer drug delivery.

2. Materials and methods

2.1. Materials

The citric acid was supplied by Chem-lab (Belgium). Urea, ethylenediaminetetraacetic, bicarbonate sodium, L-glutamine, Penicillin/Streptomycin and Insulin were purchased from Merck (Germany). Hydrochloric acid was supplied by Neutron Pharmachemical Co manufacturer (Iran), Sodium hydroxide was obtained from Biochem Chemopharma Company (France) the Roswell Park Memorial Institute (RPMI). 1640 and fetal bovine serum (FBS) were supplied by Gibco Invitrogen (USA), MCF-7 cell line was provided by Pasteur Institute cell bank (Iran).

2.2. Synthesis of CQD

To prepare N-doped CQD, at first, 1.0 g of citric acid and 1.0 g urea were dissolved in 50 mL distilled water (40 mg/mL) under continuous stirring to obtain a clear solution. The solution was then transferred into a hydrothermal reactor (150 mL) and was heated for 8 h in the oven at 180 °C [13]. The resulting solution was then allowed to cool down to room temperature, followed by pH neutralization from the initial pH of about 8.7, through careful dropwise adding of 10 M NaOH to the solution under rigorous stirring. After centrifuging the solution to separate larger particles (20,000 rpm, 30 min), the synthesized CQDs were purified by dialysis bag (molecular-weight cutoff: 10 kDa) against deionized water under constant stirring for 24 h.

2.3. Drug loading

10 mg CQD was sonicated for 12 min, at room temperature, in 8 mL of deionized water, followed by the addition of 2 mL of MTX solution (0.35 mg/mL). The suspension was mixed at room temperature for 30 min, then centrifuged (20,000 rpm, 30 min). The supernatant was collected for analysis. The amount of unbound MTX in the supernatant was evaluated for the measurement of drug loading [14].

In this regard, considering the half maximal Inhibitory Concentration (IC_{50}) of the free MTX, some known concentrations of 0.002, 0.004, 0.008, 0.0175, 0.035 mg/mL of MTX drug were prepared. The absorption of these MTX concentrations at 608 nm wavelength

were recorded by enzyme-linked immunosorbent assay (ELISA) reader (Infinite, M200 PRO, Tecan, USA). The absorption wavelength of 608 nm is specific to the drug and none of the other components of the complex absorb at this specific wavelength. Using the data, a standard MTX curve was generated whereby a graph of drug concentration versus absorbance was plotted. The line equation was achieved, as shown below (Eq. 2.1). Moreover, the percentage of DEE was calculated according to Eq. 2.2.

$$\text{Absorbance (a.u.)} = 21.923 \times (\text{Drug concentration in mg / mL}) + 0.0375 \tag{2.1}$$

$$\text{DEE (\%)} = \text{Drug concentration in the complex / Initial drug concentration} \times 100 \tag{2.2}$$

2.4. Characterization of particles

2.4.1. Photoluminescence

Photoluminescence investigation of CQD was performed by UV–Vis Spectroscopy (the PerkinElmer LS45, Massachusetts, USA). In order to investigate the photoluminescence of the CQD in acidic, neutral and basic pH, the pH of the CQD was adjusted from 4 to 9. The emission intensity of the CQDs at different pH values was recorded by dropping CQDs with each prepared pH on filter paper, therefore, making fluorescent spots. In order to capture images from the samples, the INTAS Gel documentation hood imager (Göttingen, Germany) was used to photograph the CQD emissions. Images were analyzed using the Image J software (1997).

2.4.2. Dynamic light scattering measurement

The size distribution of CQD and CQD-MTX complex were determined by dynamic light scattering (DLS) method using Malvern Nano ZS (England). The surface charges of particles (zeta-potential) were measured under an electric field using this instrument.

2.4.3. Transmission electron microscopy

The bright-field high resolution transmission electron microscopy (HR-TEM) was conducted to analyze the morphology and particle size of CQD. In this regard, CQD specimen was diluted in distilled water and the suspension was then homogenized (ultrasonic bath, 5 min). Immediately after the ultrasonic treatment, micro-droplets were put onto 3 mm lacey carbon TEM grids (TED PELLA INC.) and left to dry for at least 30 min. Afterwards, the grids containing the CQDs were analyzed in a JEOL 2200FS TEM (Tokyo, Japan) at 200 kV [15].

2.4.4. Fourier transform infrared spectroscopy

Fourier transform infrared (FTIR) spectroscopy (Thermo Nicolet model NEXUS 470, Illinois, USA), a powerful tool to reveal structural information such as functional groups, was performed to evaluate the structural properties of synthesized products. Specimens were dried to a powder before each analysis.

2.5. In vitro drug release study

Drug release investigation was performed in 50 mL phosphate-buffered saline (PBS) at pH 7.4 and 5.2 during 48 h. Also, diffusion investigation was performed for the free drug and the CQD-MTX complex at pH 7.4 within 6 h. At first, the CQD-MTX complex was poured in a dialysis bag (molecular-weight cutoff: 10 kDa) and placed inside a beaker containing PBS. Then, at specific time intervals, aliquots of the buffer solution were collected to record drug release using ELISA reader at a wavelength of 608 nm. The percentage of MTX cumulative release was calculated using the following equation, Eq. 2.3.

$$\textit{Cumulative release (\%)} = \textit{Amount of drug released from complex / Amount of drug in the PBS} \times 100 \tag{2.3}$$

In addition, the free MTX diffusion investigation was performed with a concentration equal to 0.34 mg/mL, using the same technique to compare the cumulative release rate of free MTX and CQD-MTX complex. Finally, similar to the previous technique, the percentage of cumulative release of free MTX was calculated using the formula Eq. 2.3.

2.6. In vitro cell viability evaluation

Briefly, the MCF-7 cells were cultured in RPMI1640 medium, which is supplemented with 15 % FBS, 10 g/mL of insulin, 100 g/mL of streptomycin, 100 U/mL of penicillin and 2 % L-glutamine under 5 % CO_2 atmosphere at 37 °C. As a control, the cell line of MCF-7 was also cultured in RPMI1640 medium.

In order to evaluate the toxicity on MCF-7 cell of free MTX, CQD-MTX complex and CQD in different concentrations, the cytotoxicity test was performed using the Methylthiazolyldiphenyl-tetrazolium bromide (MTT) assay. Initially, the cultured cells were transferred to a 96-well plate, where 100,000 cells were cultured in each well and incubated at 37 °C in an atmosphere containing 5 % CO_2 gas for two days. Cells were allowed to stick to the bottom of the wells and the supernatant was removed. Subsequently, the cells were incubated with varying concentrations of 0.15, 0.3, 0.5, 0.8, 1.2, 2.5 μM free MTX, CQD-MTX complex and CQD for 2 and 5 h. 100 μl of MTT was then added at a concentration of 5 mg/mL to each well and the cells were incubated for another 4 h. In fact, when MTT enters the cells, it leads to the formation of insoluble formazan crystals. The formazan crystals were completely dissolved by 100 μL/well of DMSO and the absorbance value of each well was evaluated by the ELISA microplate reader at a wavelength of 540 nm. Utilizing Eq. 2.4, the cell viability of MCF-7 cells was calculated.

$$\textit{Cell viability}\ (\%) = \textit{Absorption of the treated cells}/\textit{Absorption of untreated cells}\ (\textit{Control absorption}) \times 100 \quad (2.4)$$

2.7. Antioxidant test

In order to determine the antioxidant activities of the CQD and CQD-MTX complex, the antioxidant test was performed by ferric-reducing antioxidant power assay using a commercial standard kit (Naxifer™, Navand Salamat). At first, concentrations of 0, 0.1, 0.2, 0.3, 0.4, 0.5 mM of Trolox, a water-soluble vitamin E analog, were used as antioxidant standards to prepare the standard curve (Fig. S3). The antioxidant activity of CQD and CQD-MTX complex depended on the reduction of colorless ferric-tripyridyltriazine (Fe^{3+}-TPTZ) to an intense blue-colored ferrous-tripyridyltriazine complex (Fe^{2+}-TPTZ) which is measured at 593 nm. The antioxidant activity of CQD and CQD-MTX complex was expressed as mmol Fe^{2+} per mg.

2.8. Statistical analysis

All measurements were performed in triplicate and results are presented as mean ± standard deviation. Also, differences with p-value <0.05 were considered significant by statistical analysis.

3. Results

3.1. Characterization of CQD

In the study of the size and size distribution of the CQD, HR-TEM and DLS techniques were employed. The HR-TEM image of N-doped CQDs showed a rather uniform distribution of CQDs with an average diameter 36.78 ± 0.9 nm, as also confirmed by DLS results (Fig. 1a and b). The zeta-potential results indicated a surface charge potential of −0.722 ± 0.4 mV.

The photoluminescence characteristics for the N-doped CQD, revealed a maximum absorption peak at 360 nm and, the emission spectra show maximum intensity at 420 nm (Fig. 2a). In addition, after investigating the effect of pH on photoluminescence of CQD, the maximum fluorescence intensity was obtained at pH 6 and 7 (Fig. 2b), showing that the CQD-MTX complex can be considered as a trackable drug delivery agent with sustained photoluminescence in tumor and healthy cell environments, respectively.

Chemical bond absorption pattern of the CQD and MTX drug were obtained using the FTIR spectrum. The FTIR spectrum of the N-doped CQD demonstrated a broad stretching bond at 1060 cm^{-1} that was related to the carboxylic bonds and aromatic bonds (C═C) identified at approximately 1450 cm^{-1}. Amide bonds were observed between 1600 to 1700 cm^{-1}. Amine functional groups revealed vibrations ranging from 3485 to 3560 cm^{-1} wavenumbers (Fig. 3a) [13]. The MTX drug had a C–O stretching at 1215 cm^{-1}, the aromatic bond C═C were identified between 1500 to 1607 cm^{-1}. The hydroxyl (O–H) and amine functional groups were also observed at 3148 cm^{-1} (Fig. 3b) [3].

3.2. Characterization of the CQD-MTX complex

The CQD-MTX complex represented a size distribution of 157.8 ± 12.18 nm, according to HR-TEM and DLS results (Fig. 4a and b). The zeta-potential results indicated that the CQD-MTX complex had a positive surface charge of 0.718 ± 0.1 mV.

In order to compare the characteristic absorptions of the chemical bonds in the CQD, MTX and CQD-MTX complex, FTIR spectrum of the complex was obtained. The FTIR of CQD-MTX complex showed both the characteristic peaks of CQD and MTX. Based on the FTIR

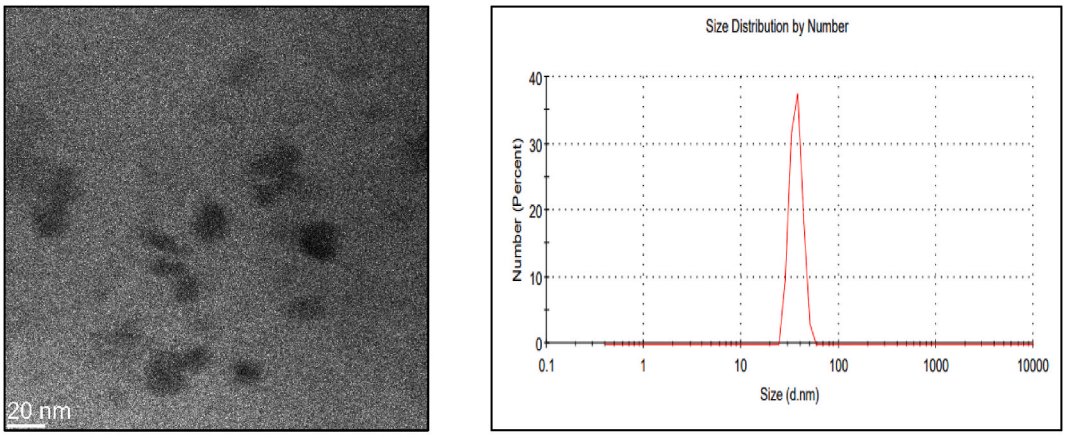

Fig. 1. The results of HR-TEM and DLS of CQDs.

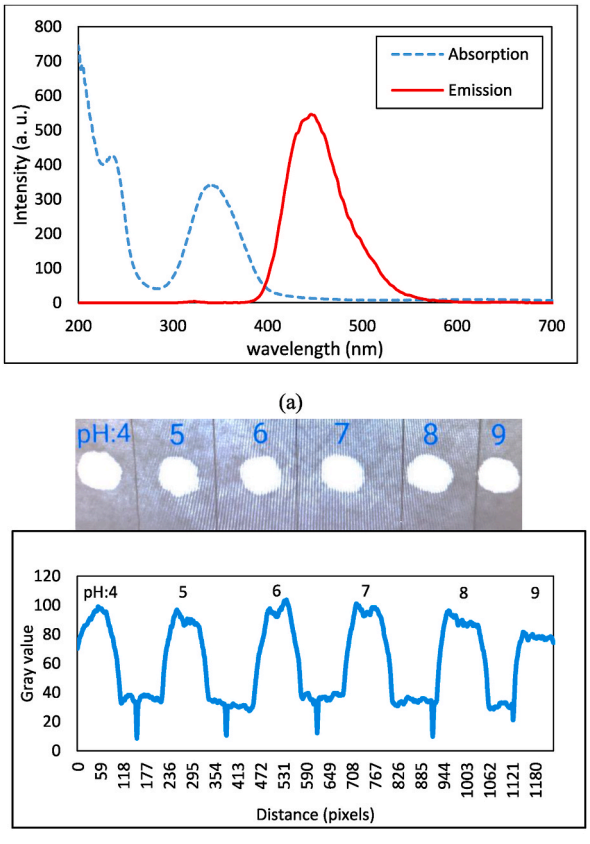

Fig. 2. The results of photoluminescence: (a) absorption and emission spectroscopy diagram and, (b) the effect of pH on the emission of CQD.

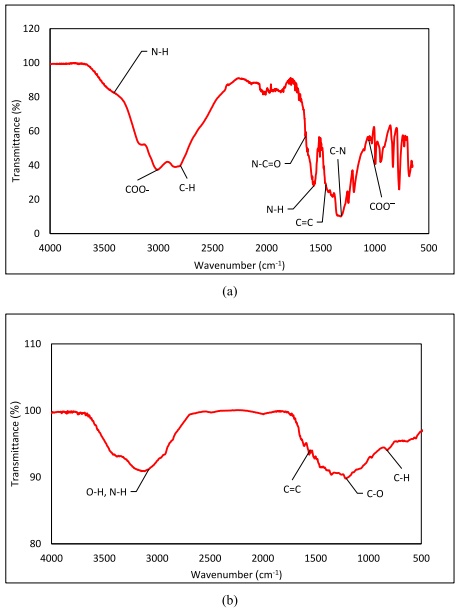

Fig. 3. From top to bottom FTIR images of: (a) CQD and, (b) MTX.

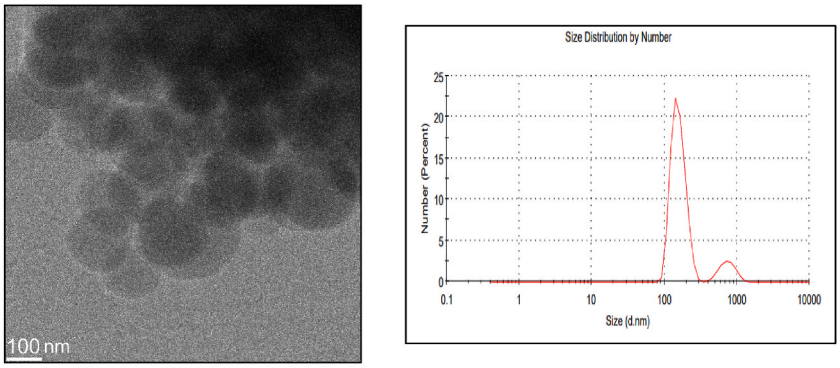

(a) (b)

Fig. 4. The results of HR-TEM and DLS of CQD-MTX complex.

results, due to the loading of MTX, the C–O stretching peak of MTX (Fig. 3b) shifted from 1215 to 1292 cm^{-1} and the aromatic bond (C═C) also changed in wavenumber from 1560 to 1662 cm^{-1} (Fig. 5). These shifts highlight the successful loading of MTX onto CQD.

3.3. Determination of DEE

A standard curve of MTX and its related line equation (Eq. 2.1) were obtained (Fig. S2). Utilizing them, the drug concentration was determined in the complex, and the percentage of DEE was calculated to be 97 % using Eq. 2.2, revealing a high amount of DEE.

3.4. In vitro drug release profile

The 48-h drug release profile of MTX at pH 7.4 and 5.2 from CQD-MTX complex, and the 6-h drug diffusion for free MTX were analyzed in 50 mL PBS (Fig. 6a and b). Based on the measurements, the comparison of the results of drug release and diffusion rates shows a significant controlled drug release for the system in 6 h, creating a sustained and reduced drug-diffusion profile at initial hours (Fig. 6a). In addition, the cumulative release of MTX from CQD-MTX complex (Fig. 6b) was 8 % at pH 7.4 and 11 % at pH 5.2, after 48 h, whereas in case of free drug, approximately 77 % of free MTX was released after 6 h. In order to obtain the error bars for each curve (Fig. 6a and b), the cumulative release was calculated utilizing Eq. 2.3 in triplicate.

3.5. In vitro cell cytotoxicity

MTT evaluation was performed to investigate the cytotoxicity at different concentrations of free MTX, CQD-MTX complex and CQD on MCF-7 cells after 2 h (Fig. 7a) and 5 h (Fig. 7b). According to Fig. 7a and b, in the case of free MTX, a strong cytotoxic effect was achieved in a short time, and this effect was further enhanced along with decreased cell viability, which is a positive correlation with respect to incubation time and concentration. The cell viability of MCF-7 cells incubated with CQD-MTX complex decreased with increasing MTX concentration. It should be noted that the cytotoxic effect of CQD-MTX complex for MCF-7 cells was reduced relative to the free MTX at different concentrations of MTX after 2 h and 5 h of treating, which can be concluded that the increase in cell viability was mainly caused by the gradual release of MTX from CQD. According to Fig. 7c, after 5 h of treating, due to the better fit of the data with line at the concentration of 0.5 ± 0.17 μM, the optimal gradual release of MTX from the CQD-MTX complex was obtained at this concentration. In addition, it was found that CQD had no significant effect on inhibition of cell growth. Also, the percentages of cell viability were obtained using Eq. 2.4, followed by IC_{50} values, and based on the results, the IC_{50} for free MTX was obtained at a concentration between 0.3 to 0.5 μM after 5 h of treating while for CQD-MTX complex, it was achieved between 0.5 to 0.8 μM after 5 h

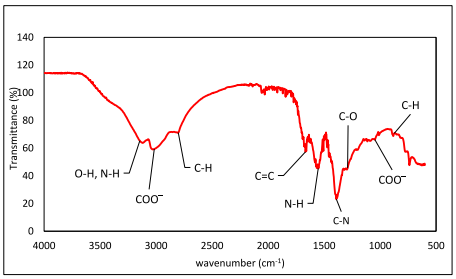

Fig. 5. FTIR image of CQD-MTX complex.

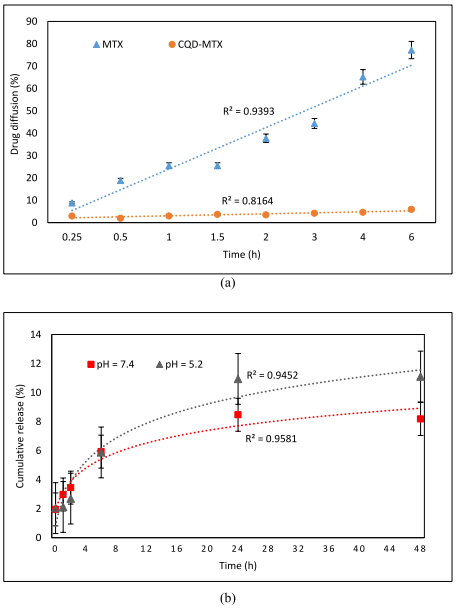

Fig. 6. (a) Drug release from CQD-MTX complex compared to the diffusion of free MTX at pH 7.4 within 6 h and, (b) drug release from CQD-MTX complex at pH 7.4 and pH 5.2 after 48 h. The error bars for each curve represent standard deviations achieved from three replications.

(Fig. 7b). Differences with p-value <0.05 were determined significant by statistical analysis.

3.6. Antioxidant test

Commonly, antioxidant activity is a parameter used to evaluate the ability of a compound to scavenge and neutralize free radicals. In reference to the fitted curve shown in Fig. 8, the antioxidant activity of CQD was investigated at different concentrations. It was found that the CQDs had an antioxidant activity, that reduces linearly with the dilution of the CQDs ($R^2 = 0.94$). In effect, the antioxidant activity of CQD-MTX complex was observed. The total antioxidant capacity of CQD-MTX complex was calculated 0.06 ± 0.01 mmol Fe^{2+}/mg by utilizing the obtained equation from the standard curve (Fig. S3), showing that the incorporation of CQD as a carrier would lead to improved effectiveness of the treatment.

4. Discussion

Chemotherapy has been the main modality of treatment for cancer patients; however, its success rate remains low. The poor accessibility of anticancer agents that target the tumor, the requirement of higher doses, and the nonselective nature of these agents, leads to severe toxicity in healthy cells. Thus, targeted drug delivery holds immense potential to improve the treatment of cancer by selectively providing therapeutically effective drug concentrations at the tumor site [16]. Nanotechnology-based cancer therapeutics and drug delivery systems are highly used for enhancing drug solubility, stability, safety, as well as decreasing multidrug resistance [17]. Amongst compound carriers, the CQD, a quantum-sized carbon material, has gained great attention as a novel material primarily due to its excellent hydrophilicity, low toxicity and good biocompatibility properties [18,19]. Furthermore, the small size of N-doped CQDs is a desirable feature due to factors such as high surface area, greater contact with surrounding materials and accessibility to target areas such as drug delivery agents, N-doped CQDs were successfully used to target MCF-7 and HeLa cancer cells along with doxorubicin drug, exhibiting pH-dependent release, which can reduce the side effects of the chemotherapeutic drug on normal cells [20–22].

Based on studies, MTX is a type of anti-cancer drug that inhibits DNA replication and RNA transcription and it also affects the cell cycle at different stages [23]. In this research, N-doped CQD was synthesized via a hydrothermal method, followed by purification using dialysis that also resulted in uniform distribution of CQDs. The synthesis conditions, such as temperature, solvent, and precursors, are known to significantly affect the properties of fabricated CQDs, including their optical features, toxicity, and catalytic behavior. Since the CQDs synthesized in this study were expected to be used for biomedical applications, hydrothermal method was used, which involves the reaction of small-sized organic compounds in a solvent at high temperatures to fabricate biocompatible sub-10-nm CQDs [24].

In this study, the percentage of DEE of CQD-MTX complex was calculated, and the cumulative release of MTX from CQD-MTX complex was investigated at pH 7.4 and 5.2 after 48 h. Based on the results, the percentage of DEE of CQD-MTX complex was obtained 97 %, while, in studies conducted by Hashemi *et al.* and Wang *et al.*, the percentages of DEE of prepared complexes were 68 %, 91.36 %, respectively [3,9]. In addition, in this research, the cumulative release of MTX from CQD-MTX complex was 8 % and 11 % at

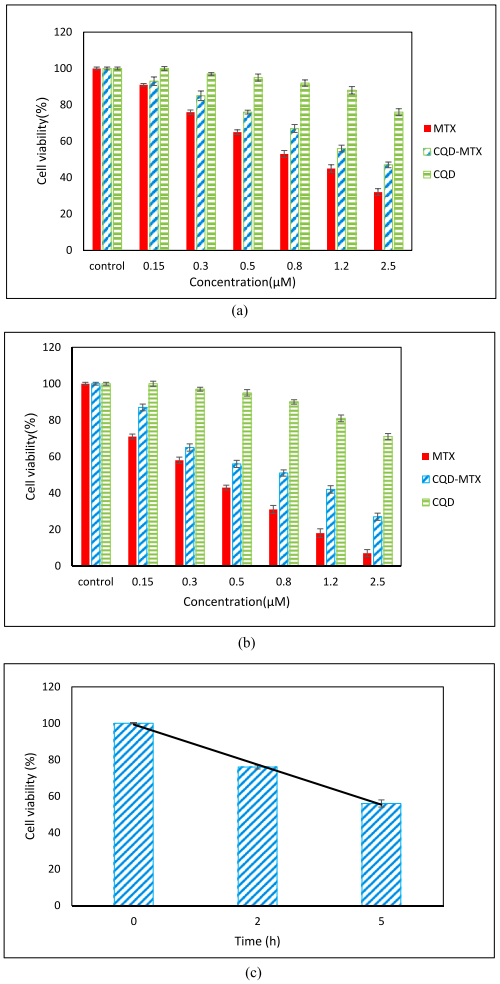

Fig. 7. The graph obtained from the MTT evaluation after (a) 2 h and, (b) 5 h; and (c) the optimal gradual release of MTX from the CQD-MTX complex at concentration of 0.5 μM after 5 h. The error bars for each curve represent standard deviations achieved from three replications of measurement.

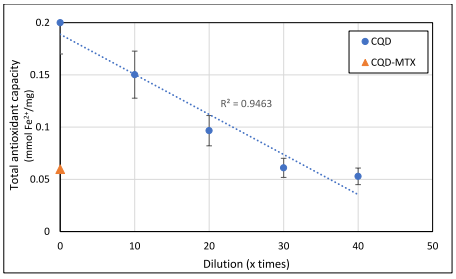

Fig. 8. A curve prepared from the antioxidant activity of CQD and CQD-MTX complex. The error bars for each curve represent standard deviations achieved from three measurements of the same sample.

pH 7.4 and 5.2 after 48 h, respectively, while, in study conducted by Darvish *et al.*, the percentages of released MTX from chitosan-MTX after 48 h were about 45 % and 67 % at pH 7.4 and 5.2, respectively. Moreover, the release rates from chitosan-hexagonal gold-MTX after 48 h were 34 % and 55 % at pH 7.4 and 5.2, respectively [10].

The zeta-potential measurement determined the surface charges of CQD was negative and because of the positive surface charge of MTX drug, after the loading of MTX drug to CQD, the CQD-MTX complex had a positive surface charge, which implies an electrostatic interaction between the MTX drug and CQD, which had the greatest effect on the pH-dependent drug release behavior. In fact, the

strength of electrostatic interaction between the MTX drug and CQD changes by alteration of the pH, including decreasing OH^- ion and increasing H^+ ion at acidic environment, as a result, an increase in the drug release is obtained [25].

Based on the data obtained from release and diffusion investigation, it can be determined that the incorporation of CQD and MTX had a significant effect on maintaining and controlling the release of the drug in the physiologic environment of pH 7.4. An acidic pH, such as the environment of the cancer cells, increased drug release. These results show an improvement in the pharmacokinetic properties of the drug, mainly due to an alteration in its distribution and absorption parameters.

Based on the results of the MTT evaluation, the IC_{50} was obtained for the CQD-MTX complex at a concentration between 1.2 and 2.5 μM after 2 h (Fig. 7a), while in another study, the IC_{50} value for breast cancer cells treated with hollow gold nanostructure-PEG-MTX was 2.13 μM after 1.5 h [26]. On the other hand, by examining the cytotoxicity effect of CQD on cancer cells, no significant toxicity was found, as a result the CQD was used as a powerful tool in targeted drug delivery. However, it is important to note that CQDs have shown moderate anti-cancerous properties when exposed for a longer duration, in the presence of anticancer drugs [27]. Therefore, further research is needed to fully understand the cytotoxic effects of CQDs on normal and cancerous cells, at different exposure duration, in or without the presence of anticancer drugs to gain a better insight on their more advanced potential applications in biomedicine, and their role in inhibiting oxidative stresses in cancerous cells by preventing the aggregation of Fe^{3+} ions through their antioxidant properties [28,29].

Iron is a transition metal that has a significant role in catalyzing the production of free radicals. Aggregation can promote oxidative stresses. Chelating agents can bind and separate free Fe^{3+} ions, preventing them from contribute to oxidative reactions. Furthermore, by chelating Fe^{3+}, compounds can prevent free radical formation [28]. This is an important mechanism behind their antioxidant properties. Based on the results obtained from the antioxidant test, the antioxidant activity of CQDs plays a significant role in their biomedical applications, such as drug delivery (Fig. 8), where Reactive oxygen species generation can disrupt the process of cell [29]. Moreover, in a previous study, it was reported that curcumin acts as a potent antioxidant agent [30], and based on the studies performed by Hashemi *et al.*, curcumin loaded in PLGA nanoparticles improved anticancer efficiency of MTX on MCF-7 cells similar to this study's CQD-MTX complex results [31].

5. Conclusion

New targeted drug delivery approaches that are being explored using different nanosystems provide an optimistic outlook in developing successful cancer drug therapy. CQDs are emerging carbon-based nanomaterials and they are receiving considerable interest in biomedical applications including targeted drug delivery. In this investigation, the CQD was studied to interact with MTX to form CQD-MTX complex. After drug loading, the percentage of DEE was 97 % and the characterization of the CQD and CQD-MTX complex, showed that the interaction between the CQD and the MTX drug was electrostatic. Moreover, the drug release investigation, showed that the cumulative release of MTX from CQD-MTX complex was slightly higher in an acidic environment after 2 days (8 % at pH 7.4 and 11 % at pH 5.2 after 48 h), while the cumulative release of the free MTX was high at neutral pH after a short analysis time (77 % at pH 7.4 after 6 h). The results of MTT showed that after 5 h of treatment on cancer cells, maximal inhibition of the growth of MCF-7 cells was achieved at the CQD-MTX complex concentration of 2.5 μM, while the CQD had no significant effect on inhibition of cell growth. Finally, the antioxidant test of the CQD-MTX complex, revealed that the CQD can be considered as a suitable candidate for delivery of MTX drug.

Data availability

Data will be made available on request.

CRediT authorship contribution statement

Shahrzad Raeispour: Writing – original draft, Data curation. **Moones Rahmandoust:** Writing – review & editing, Supervision, Resources, Project administration, Methodology, Investigation, Conceptualization. **Hasan Kouchakzadeh:** Writing – review & editing, Supervision, Resources, Project administration, Methodology, Investigation, Conceptualization.

Declaration of competing interest

The authors declare that they have no known competing financial interests or personal relationships that could have appeared to influence the work reported in this paper.

Acknowledgements

The research was not funded.

Appendix A. Supplementary data

Supplementary data to this article can be found online at https://doi.org/10.1016/j.heliyon.2024.e31674.

References

[1] A. Stanisławek, Breast cancer—epidemiology, risk factors, classification, Prognostic Markers, and Current Treatment Strategies— An Updated Review (2021) 1–30.

[2] Y.N. Ertas, K.A. Dorcheh, A. Akbari, E. Jabbari, Nanoparticles for targeted drug delivery to cancer stem cells: a review of recent advances, Nanomaterials 11 (2021), https://doi.org/10.3390/nano11071755.

[3] C. Wang, M. Han, X. Liu, S. Chen, F. Hu, J. Sun, H. Yuan, Mitoxantrone-preloaded water-responsive phospholipid-amorphous calcium carbonate hybrid nanoparticles for targeted and effective cancer therapy, Int. J. Nanomed. 14 (2019) 1503–1517, https://doi.org/10.2147/IJN.S193976.

[4] Z. Li, J. Fan, C. Tong, H. Zhou, W. Wang, B. Li, B. Liu, W. Wang, A smart drug-delivery nanosystem based on carboxylated graphene quantum dots for tumor-targeted chemotherapy, Nanomedicine 14 (2019) 2011–2025, https://doi.org/10.2217/nnm-2018-0378.

[5] M. Sharifi, W.C. Cho, A. Ansariesfahani, R. Tarharoudi, H. Malekisarvar, S. Sari, S.H. Bloukh, Z. Edis, M. Amin, J.P. Gleghorn, T.L.M. Ten Hagen, M. Falahati, An updated review on EPR-based solid tumor targeting nanocarriers for cancer treatment, Cancers 14 (2022) 1–17, https://doi.org/10.3390/cancers14122868.

[6] X. Li, K. Vinothini, T. Ramesh, M. Rajan, A. Ramu, Combined photodynamic-chemotherapy investigation of cancer cells using carbon quantum dot-based drug carrier system, Drug Deliv. 27 (2020) 791–804, https://doi.org/10.1080/10717544.2020.1765431.

[7] Y.Z. Bu, J.R. Xu, Q. Luo, M. Chen, L.M. Mu, W.L. Lu, A precise nanostructure of folate-overhung mitoxantrone dna tetrahedron for targeted capture leukemia, Nanomaterials 10 (2020), https://doi.org/10.3390/nano10050951.

[8] M.A. El-Emam, S. El Achy, D.M. Abdallah, H.S. El-Abhar, M.A. Gowayed, Does physical exercise improve or deteriorate treatment of multiple sclerosis with mitoxantrone? Experimental autoimmune encephalomyelitis study in rats, BMC Neurosci. 23 (2022) 1–17, https://doi.org/10.1186/s12868-022-00692-1.

[9] M. Hashemi, K. Abnous, S. Balarastaghi, N. Hedayati, Z. Salmasi, R. Yazdian-Robati, Mitoxantrone-loaded PLGA nanoparticles for increased sensitivity of glioblastoma cancer cell to TRAIL-induced apoptosis, J. Pharm. Innov. 17 (2022) 207–214, https://doi.org/10.1007/s12247-021-09551-8.

[10] W. Darwish, R.A. Lafta, M.W. Shafaa, M.S. El-Nagdy, Mitoxantrone in synergism with gold hexagonal nanoparticles and gamma radiation for effective treatment of MCF7 cells, Egypt, J. Chem. 65 (2022) 639–647, https://doi.org/10.21608/ejchem.2021.86310.4185.

[11] A. Dias-Carvalho, A. Margarida-Araújo, A. Reis-Mendes, C.O. Sequeira, S.A. Pereira, P. Guedes de Pinho, F. Carvalho, S.I. Sá, E. Fernandes, V.M. Costa, A clinically relevant dosage of mitoxantrone disrupts the glutathione and lipid metabolic pathways of the CD-1 mice brain: a metabolomics study, Int. J. Mol. Sci. 24 (2023), https://doi.org/10.3390/ijms241713126.

[12] O.Y. Selyutina, S.V. Babenko, I.A. Slepneva, N.E. Polyakov, G.J. Kontoghiorghes, Increased free radical generation during the interaction of a quinone-quinoline chelator with metal ions and the enhancing effect of light, Pharmaceuticals 16 (2023), https://doi.org/10.3390/ph16081116.

[13] M. Yazdani, M. Rahmandoust, H. Kouchakzadeh, Development of various carbon nanoparticles and albumin complexes for potential theranostics applications, J. Drug Deliv. Sci. Technol. 77 (2022) 103901, https://doi.org/10.1016/j.jddst.2022.103901.

[14] A. Borhan, D.D. Herea, D. Gherca, C. Stavila, A.E. Minuti, M. Grigoras, C.M. Danceanu, L. Labusca, G. Stoian, G. Ababei, C. Stan, N. Lupu, H. Chiriac, Flash-cooling assisted sol-gel self-ignited synthesis of magnetic carbon dots-based heterostructure with antitumor properties, Mater. Sci. Eng. C. 117 (2020) 111288, https://doi.org/10.1016/j.msec.2020.111288.

[15] S. Zoghi, M. Rahmandoust, A novel technique to overcome fluid flow influence in carbon quantum dots/paper-based analytical devices, Sci. Rep. 12 (2022) 1–10, https://doi.org/10.1038/s41598-022-22837-2.

[16] J. Li, Q. Wang, G. Xia, N. Adilijiang, Y. Li, Z. Hou, Z. Fan, J. Li, Recent advances in targeted drug delivery strategy for enhancing oncotherapy, Pharmaceutics 15 (2023), https://doi.org/10.3390/pharmaceutics15092233.

[17] U. Hani, M. Rahamathulla, R.A. Osmani, H.Y. Kumar, D. Urolagin, M.Y. Ansari, K. Pandey, K. Devi, S. Yasmin, Recent advances in novel drug delivery systems and approaches for management of breast cancer: a comprehensive review, J. Drug Deliv. Sci. Technol. 56 (2020) 101505, https://doi.org/10.1016/j.jddst.2020.101505.

[18] C. Huang, H. Dong, Y. Su, Y. Wu, R. Narron, Q. Yong, Synthesis of carbon quantum dot nanoparticles derived from byproducts in bio-refinery process for cell imaging and in vivo bioimaging, Nanomaterials 9 (2019), https://doi.org/10.3390/nano9030387.

[19] N. Mahmoudi, F. Fatemi, M. Rahmandoust, F. Mirzajani, S.O. Ranaei Siadat, Development of a carbon quantum dot-based sensor for the detection of acetylcholinesterase and the organophosphate pesticide, Heliyon 9 (2023) e19551, https://doi.org/10.1016/j.heliyon.2023.e19551.

[20] K. Soumya, N. More, M. Choppadandi, D.A. Aishwarya, G. Singh, G. Kapusetti, A comprehensive review on carbon quantum dots as an effective photosensitizer and drug delivery system for cancer treatment, Biomed. Technol. 4 (2023) 11–20, https://doi.org/10.1016/j.bmt.2023.01.005.

[21] W. Bao, H. Ma, N. Wang, Z. He, pH-sensitive carbon quantum dots−doxorubicin nanoparticles for tumor cellular targeted drug delivery, Polym. Adv. Technol. 30 (2019) 2664–2673, https://doi.org/10.1002/pat.4696.

[22] M. Frieler, C. Pho, B.H. Lee, H. Dobrovolny, A.V. Naumov, G.R. Akkaraju, Effects of doxorubicin delivery by nitrogen-doped graphene quantum dots on cancer cell growth: experimental study and mathematical modeling, Nanomaterials 11 (2021) 1–15, https://doi.org/10.3390/nano11010140.

[23] Z. Chen, S. Li, F. Li, C. Qin, X. Li, G. Qing, J. Wang, B. Xia, F. Zhang, L. Meng, X.J. Liang, Y. Xiao, DNA damage inducer mitoxantrone amplifies synergistic mild-photothermal chemotherapy for TNBC via decreasing heat shock protein 70 expression, Adv. Sci. 10 (2023) 1–13, https://doi.org/10.1002/advs.202206707.

[24] V. Magesh, A.K. Sundramoorthy, D. Ganapathy, Recent advances on synthesis and potential applications of carbon quantum dots, Front. Mater. 9 (2022) 1–27, https://doi.org/10.3389/fmats.2022.906838.

[25] Q. Duan, J. Shi, L. Zhou, B. Zhang, X. Wang, S. Sang, pH-responsive and sustained release drug delivery system of BSA coated CDs-DOX, J. Mol. Struct. 1248 (2022) 131358, https://doi.org/10.1016/j.molstruc.2021.131358.

[26] V. Abolzadeh, A. Imanparast, H. Nassirli, N.T. Meybodi, B.K. Najafabad, A. Sazgarnia, In vivo evaluation of Sono-chemo therapy via hollow gold nanoshells conjugated to mitoxantrone on breast cancer, Iran, J. Basic Med. Sci. 26 (2023) 285–294, https://doi.org/10.22038/IJBMS.2023.67602.14811.

[27] K. Naik, S. Chaudhary, L. Ye, A.S. Parmar, A strategic review on carbon quantum dots for cancer-diagnostics and treatment, Front. Bioeng. Biotechnol. 10 (2022) 1–21, https://doi.org/10.3389/fbioe.2022.882100.

[28] S. Islam, N. Hoque, N. Nasrin, M. Hossain, F. Rizwan, K. Biswas, M. Asaduzzaman, S. Rahman, D.W. Hoskin, S. Sultana, C. Lehmann, Iron overload and breast cancer: iron chelation as a potential therapeutic approach, Life 12 (2022), https://doi.org/10.3390/life12070963.

[29] Ł. Janus, J. Radwan-Pragłowska, M. Piatkowski, D. Bogdał, Smart, tunable CQDs with antioxidant properties for biomedical applications—ecofriendly synthesis and characterization, Molecules 25 (2020), https://doi.org/10.3390/molecules25030736.

[30] C. Xu, M. Wang, B. Zandieh Doulabi, Y. Sun, Y. Liu, Paradox: curcumin, a natural antioxidant, suppresses osteosarcoma cells via excessive reactive oxygen species, Int. J. Mol. Sci. 24 (15) (2023) 11975. https://doi.org/10.3390/ijms241511975.

[31] M. Hashemi, Z. Haghgoo, R. Yazdian-Robati, S. Shahgordi, Z. Salmasi, K. Abnous, Improved anticancer efficiency of Mitoxantrone by Curcumin loaded PLGA nanoparticles targeted with AS1411 aptamer, Nanomedicine J. 8 (2021) 21–29, https://doi.org/10.22038/nmj.2021.08.03.